Atmospheric
Chemistry
and Physics

Impact of international shipping emissions on ozone and PM$_{2.5}$ in East Asia during summer: the important role of HONO and ClNO$_2$

Jianing Dai and Tao Wang

Department of Civil and Environmental Engineering, The Hong Kong Polytechnic University,
Hong Kong SAR, 999077, China

Correspondence: Tao Wang (cetwang@polyu.edu.hk)

Abstract. Ocean-going ships emit large amounts of air pollutants such as nitrogen oxide (NO$_x$) and particulate matter. NO$_x$ emitted from ships can be converted to nitrous acid (HONO) and nitryl chloride (ClNO$_2$), which produce hydroxyl (OH) and chlorine (Cl) radicals and recycle NO$_x$, thereby affecting the oxidative capacity and production of secondary pollutants. However, these effects have not been quantified in previous investigations of the impacts of ship emissions. In this study, a regional transport model (WRF-Chem) revised to incorporate the latest HONO and ClNO$_2$ processes was used to investigate their effects on the concentrations of RO$_x$ (RO$_2$ + HO$_2$ + OH) radicals, ozone (O$_3$), and fine particulate matter (PM$_{2.5}$) in Asia during summer. The results show that the ship-derived HONO and ClNO$_2$ increased the concentration of RO$_x$ radicals by approximately 2–3 times in the marine boundary layer. The enhanced radicals then increased the O$_3$ and PM$_{2.5}$ concentrations in marine areas, with the ship contributions increasing from 9 % to 21 % and from 7 % to 10 % respectively. The largest RO$_x$ enhancement was simulated over the remote ocean with the ship contribution increasing from 29 % to 50 %, which led to increases in ship-contributed O$_3$ and PM$_{2.5}$ from 21 % to 38 % and from 13 % to 19 % respectively. In coastal cities, the enhanced levels of radicals also increased the maximum O$_3$ and averaged PM$_{2.5}$ concentrations from 5 % to 11 % and from 4 %–8 % to 4 %–12 % respectively. These findings indicate that modelling studies that do not consider HONO and ClNO$_2$ can significantly underestimate the impact of ship emissions on radicals and secondary pollutants. Therefore, it is important that these nitrogen compounds be included in future models of the impact of ship emissions on air quality.

1 Introduction

Exhaust emissions from ocean-going ships affect the chemical composition of the marine atmosphere and have a significant impact on the climate, air quality, and human health (Eyring et al., 2010; Liu et al., 2016; Corbett et al., 2007; Andersson et al., 2009). The key air pollutants emitted by vessels include gases such as sulfur dioxide (SO$_2$) and nitrogen oxides (NO$_x$ = NO + NO$_2$) and particulate matter (PM) (Eyring et al., 2005; Moldanová et al., 2009). Emissions of NO$_x$ and other ozone (O$_3$) precursors, volatile organic compounds (VOCs) and carbon monoxide (CO), from shipping contribute to the tropospheric O$_3$ burden and hydroxyl radicals (OH), thereby influencing global radiative forcing and oxidative power (Lawrence and Crutzen, 1999). Ship-generated aerosols also affect the radiative budget by scattering and absorbing solar and thermal radiation directly and by altering cloud properties (Eyring et al., 2010; Fuglestvedt et al., 2009; Lawrence and Crutzen, 1999; Liu et al., 2016; Devasthale et al., 2006). Ship emissions in ports and near the coast also influence the air quality of coastal cities (Y. Zhang et al., 2017; Liu et al., 2018) and threaten public health (Liu et al., 2016; Campling et al., 2013). As international seaborne trade continues to increase, ship emissions are expected to continuously grow at a rate of 3.5 % over the 2019–2024 period (UNCTAD, 2020), and their impact on the environment is a growing concern.

The effects of ship emissions on the formation of O$_3$ and PM$_{2.5}$ have been extensively evaluated in numerical studies. On the open ocean, ship-generated NO$_x$ reacts with VOCs emitted from ships and from the background atmosphere

and enhances O_3 formation (Corbett and Fischbeck, 1997; Lawrence and Crutzen, 1999; Aksoyoglu et al., 2016; Huszar et al., 2010; Hoor et al., 2009). In coastal areas, the O_3 levels can also be increased by NO_x emitted from ships in ports and harbours and through the dispersion of ship-formed O_3 on the open ocean (Wang et al., 2019; Aksoyoglu et al., 2016; Song et al., 2010). On the other hand, ship-generated NO_x can reduce ozone formation via a titration effect in heavy-traffic ports and within the ship tracks (Wang et al., 2019; Aksoyoglu et al., 2016). Ship emissions have also been shown to increase $PM_{2.5}$ concentrations via direct emissions and via the production of secondary aerosols through the reaction of gaseous precursors (Aksoyoglu et al., 2016; Liu et al., 2018; Lv et al., 2018). Although the formation of O_3 and secondary aerosols is affected by their precursors, it can also be influenced by the levels of radicals, which are key to the oxidation of precursors. Limited attention has been paid to the production of ship-related radicals in evaluating the effects of ship emissions on secondary pollutants.

Recent studies have demonstrated the potentially important roles of two radical precursors and nitrogen reservoirs – nitrous acid (HONO) and nitryl chloride ($ClNO_2$) – in atmospheric oxidation chemistry (Fu et al., 2019; Li et al., 2016; Sarwar et al., 2014; Simon et al., 2009; L. Zhang et al., 2017). HONO is emitted directly in combustion and soil (Kleffmann et al., 2005) or is produced by heterogeneous reactions of NO_2 on various surfaces (Finlayson-Pitts et al., 2003; Ndour et al., 2008; Monge et al., 2010) and by photolysis of nitrate aerosol (Ye et al., 2017, 2016). $ClNO_2$ is formed from reactions of N_2O_5, which is produced when NO_2 reacts with O_3, on chloride-containing aerosol at night (Bertram and Thornton, 2009). Photolysis of HONO and $ClNO_2$ by sunlight produces OH or Cl radicals and recycles NO_2, thereby affecting the oxidation capacity and production of secondary pollutants (Osthoff et al., 2008; Wang et al., 2016). Ships can directly emit HONO (Sun et al., 2020), and the NO_x that they emit can subsequently produce HONO and $ClNO_2$ via heterogeneous reactions on sea-salt and ship-emitted particles. Although the production and effects of HONO and $ClNO_2$ from land-based emissions have been demonstrated over land areas (L. Zhang et al., 2017), few studies have examined the effects of the two reactive nitrogen species from international shipping. Field studies have observed elevated mixing ratios of HONO (0.2 ppb) at a marine site of the Bohai rim in northern China (Wen et al., 2019) and of HONO (126 ppt) and $ClNO_2$ (1.97 ppb) at a coastal site in southern China (Tham et al., 2014; Zha et al., 2014). These observations suggest the significant contribution of ship emissions to the oxidative capacity of the marine and coastal atmosphere in East Asia.

In this study, we used a revised regional chemical transport model to simulate the spatial distributions of HONO and $ClNO_2$ produced by ocean-going ships and their effects on the formation of O_3 and $PM_{2.5}$ in East Asia, which is home to 8 of the world's top 10 container ports and the world's most trafficked oceans. We selected the summer (July) of 2018 as the study period. During this time, large-scale oceanic winds prevailed in Asia and solar radiation and air temperature reached the highest level for the year. Thus, international shipping is expected to have the most distinctive and perhaps the greatest impact on atmospheric chemistry during this time of year in East Asia.

The remainder of the paper is structured as follows: in Sect. 2, we detail the model setting, emissions, numerical experiments, observational data, and model validation. In Sect. 3, we exhibit the model performance for HONO and $ClNO_2$ and compare the results with available measurements in marine areas; we then show the formation of ship-related HONO and $ClNO_2$ and their subsequent effects on radicals, O_3, and $PM_{2.5}$ in oceanic areas and coastal cities. Finally, our conclusions are given in Sect. 4.

2 Methodology

2.1 Model setting

In this study, the WRF-Chem model (version 3.6.1; Grell et al., 2005) with updated gases-phase and heterogeneous-phase mechanisms of new reactive nitrogen species (L. Zhang et al., 2017) was used to simulate the transport, mixing, and chemical transformation of trace gases and aerosols. Briefly, the updated module was based on the default Carbon Bond Mechanism-Z (CBMZ) module (Zaveri and Peters, 1999), in which the O_3 production came from the traditional photochemical mechanisms with only two gas-phase sources of HONO ($OH + NO \rightarrow HONO$ and $HO_2 + NO_2 \rightarrow HONO$) and no chlorine chemistry. In the updated module, CBMZ-Reactive NitrOgen Mechnism (CBMZ-ReNOM), the HONO sources included the additional gas-phase reactions between NO_x and HO_x ($OH + HO_2$); the heterogeneous reaction of NO_2 on the particle, urban, leaf (Kurtenbach et al., 2001), and sea surfaces (Zha et al., 2014); and direct emission from vehicles (Kurtenbach et al., 2001; Gutzwiller et al., 2002; Sun et al., 2020). For this study, an additional HONO source from the photolysis of particulate nitrate ($PNO_3 \rightarrow 0.67\,HONO + 0.33\,NO_2$) was included into our model. The photolysis rate constant of PNO_3 (J_{PNO_3}) was calculated following the approach used in Fu et al. (2019): $J_{PNO_3} = (8.3 \times 10^{-5}/7 \times 10^{-7}) \times J_{HNO_3\text{-WRF-Chem}}$, where $J_{HNO_3\text{-WRF-Chem}}$ is the photolysis rate constant of gaseous HNO_3 calculated online in the WRF-Chem model. For $ClNO_2$ production, the parameterization from Bertram and Thornton (2009) was used to represent the N_2O_5 uptake coefficient and $ClNO_2$ production yield. This parameterization reproduced the order of magnitude and variation in the observed N_2O_5 and $ClNO_2$ levels in a background site in Hong Kong (Dai et al., 2020). The other six chlorine species, with relevant photolysis reactions and subsequent reactions between released Cl radical and VOCs, were also added to the default module (L. Zhang et al., 2017).

The details of other chemical and physical schemes for the simulation can be found in L. Zhang et al. (2017).

The model simulations were performed from 28 June to 31 July 2018. The first 72 h of the simulations was considered spin-up time. The initial meteorological conditions were provided by reanalysis data from the Final (FNL) Operational Global Analysis dataset provided by the National Centers for Environmental Prediction (NCEP; http://rda.ucar.edu/datasets/ds083.2/, last access: 1 November 2020). The model had 31 vertical layers with a fixed top of 100 hPa. The domain covered a large part of Asia with a horizontal resolution of 36 km × 36 km (Fig. 1a). The surface layer was 30 m above the ground, and the lowest 11 layers were approximately within the height of the planetary boundary layer at noon.

2.2 Emissions

Five sets of emission inventories (EIs) were used for anthropogenic emissions in our study. For mainland China, the Multi-resolution Emission Inventory for China (MEIC; http://www.meicmodel.org/, last access: 1 November 2020) in 2016 was used. For the rest of Asia, we applied the MIX dataset (http://www.meicmodel.org/dataset-mix, last access: 1 November 2020) for 2010 (Li et al., 2017). For international shipping, the emission database in the Community Emission Data System (CEDS) (McDuffie et al., 2020) for 2017 was used. The HONO emissions from land transportation sources were calculated using their NO$_x$ emissions and the HONO/NO$_x$ ratio of 0.8 % for gasoline and 2.3 % for diesel. These commonly used ratios in model studies (Zhang et al., 2016; Fu et al., 2019) are based on the previous measurements of vehicle exhausts (Kurtenbach et al., 2001; Gutzwiller et al., 2002) and are generally consistent with more recent emission result (Liu et al., 2019; Trinh et al., 2017). For ship-emitted HONO, we set the emission ratio of HONO/NO$_x$ as 0.51 % based on the reported ratio in fresh ship plumes in Chinese waters (Sun et al., 2020). For anthropogenic chloride emissions, the high-resolution (0.1° × 0.1°) EIs of HCl and fine particulate Cl$^-$ for 2014 were applied for mainland China (Fu et al., 2018). These EIs included four sectors and have been shown to offer a reasonable model simulation of particulate chloride by the WRF-Chem model (Dai et al., 2020). The Reactive Chlorine Emission Inventory (RCEI; Keene et al., 1999) was used for anthropogenic chloride emissions in the other regions. For natural emissions, the biogenic emissions were calculated by the Model of Emission of Gas and Aerosols from Nature (MEGAN) version 2.1 (Guenther et al., 2006).

The spatial distribution of ship NO$_x$ emissions is shown in Fig. 1a. The main ship routes with high emission intensity are clearly identified in the ship emission inventory. One major shipping lane is located in the southern Bay of Bengal (BOB) in the Indian Ocean, passes through the Strait of Malacca, and extends to the South China Sea (SCS) and other

Table 1. Experimental setting.

Cases	Anth. emis.[a]	Ship emis.[b]	HONO chem.[c]	Chlorine chem.[d]
Def	Yes	Yes	No	No
Def_noship	Yes	No	No	No
Cl	Yes	Yes	No	Yes
Cl_noship	Yes	No	No	Yes
HONO	Yes	Yes	Yes	No
HONO_noship	Yes	No	Yes	No
BASE	Yes	Yes	Yes	Yes
BASE_noship	Yes	No	Yes	Yes

[a] Anthropogenic emissions except for ship emissions. [b] Ship emissions except for directly emitted HONO. [c] HONO chemistry. [d] Chlorine chemistry.

Asian countries. Distinct shipping lanes are also shown along the coast of the East China Sea (ECS) and the Sea of Japan (SOJ). Over the western Pacific Ocean (WPO), congested ship routes are distributed among Japan and other countries (Southeast Asian countries, Australia, and North America). Based on the distribution of ship NO$_x$ emissions, six water zones were selected, including three waters around China (SCS; ECS; Bohai Rim, BR), two waters in other regions (SOJ and BOB), and one open ocean (WPO; Fig. 1b). In addition, three densely populated city clusters were chosen (the North China Plain, NCP; the Yangtze River Delta, YRD; and the Pearl River Delta, PRD).

2.3 Experimental setting

Eight simulations were conducted with different emissions and chemistry, as listed in Table 1. In the Def and Def_noship cases, the WRF-Chem model was conducted with default chemistry (i.e. the default CBMZ mechanism with only the two HONO sources and no chlorine chemistry). The differences between Def and Def_noship (i.e. Def − Def_noship) represent the effects of ship emissions with the default nitrogen chemistry. In the Cl and Cl_noship cases, an updated chlorine chemistry in the revised WRF-Chem model was used. The differences between the two cases (i.e. Cl − Cl_noship) represent the effects of ship emissions with the default and additional chlorine chemistry. Similarly, in the HONO and HONO_noship cases, the additional HONO chemistry was used, and the difference between the two cases (i.e. HONO − HONO_noship) represents the default impact of ship emissions with additional HONO chemistry. In the BASE and BASE_noship cases, the integrated HONO and chlorine chemistry are considered. The differences between BASE and BASE_noship represent the shipping impact with the integrated effects of HONO and chlorine species. The results from the BASE experiment will be used to validate the model performance.
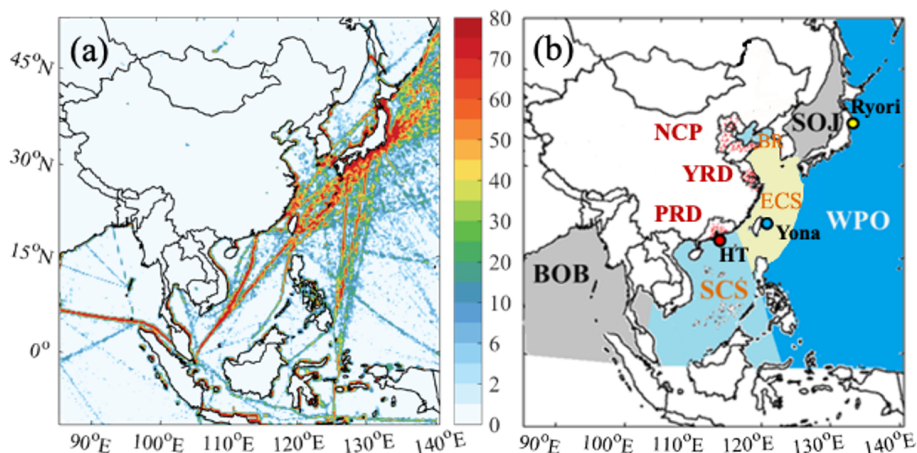
Figure 1. (a) NO$_x$ emission fluxes from ships (in g m^{-2} month^{-1}) in July 2017. **(b)** Model domains with six water zones (South China Sea, SCS; East China Sea, ECS; Bohai rim, BR; Sea of Japan, SOJ; Bay of Bengal, BOB; and western Pacific Ocean, WPO), three coastal city clusters (Pearl River Delta, PRD; Yangtze River Delta, YRD; and North China Plain, NCP), and three maritime observational sites (Hok Tsui, HT; Yonagunijima, Yona; and Ryori). Red dots in PRD, YRD, and NCP represent selected coastal sites. The ranges of latitude and longitude in each body of water are listed in Table S1 in the Supplement.

2.4 Observational data and model validation

Meteorological data from surface stations from the NOAA National Climatic Data Center (NCDC; Fig. S1a in the Supplement) comprising wind direction, wind speed, surface temperature, and specific humidity were used to validate model performance for the meteorological parameters. Conventional air pollutant data (NO$_2$, PM$_{2.5}$, and O$_3$) from surface stations (obtained from China's Ministry of Ecology and Environment; Fig. S1b) were used to evaluate the simulated air pollutants over mainland China. Table S2 summarizes the statistical performance of our model results. For meteorological parameters, high R values (> 0.85) and low mean bias (MB) values indicate good performance for the meteorological field. For regular air pollutants, the model overpredicted PM$_{2.5}$ (MB $= 10.6$ µg m^{-3}) and slightly underpredicted NO$_2$ (MB $= 3.3$ ppbv) and O$_3$ (MB $= 5.5$ ppbv). These biases in simulation can be partially explained by uncertainties in the model input, such as the land-use data (Dai et al., 2019) and emission inventory (Li et al., 2017).

The O$_3$ data from two remote sites, Ryori and Yonagunijima (Yona) in Japan (https://www.data.jma.go.jp/ghg/kanshi/ghgp/o3_e.html, last access: 1 November 2020) and one coastal background site in Hong Kong, Hok Tsui (HT), were used to compare the model performance over the maritime areas. These three sites are located along the coasts of the SCS, ECS, and WPO regions (Fig. 1b). As shown in Fig. S2, with the default chemistry, the model underpredicted the O$_3$ mixing ratio at the coastal and marine sites, with an underestimation of 2.8, 4.8, and 2.3 ppbv at the HT, Ryori, and Yona sites respectively (Table S3). With the addition of the HONO and ClNO$_2$ chemistry, the simulated O$_3$ levels at the marine sites were improved, with an MB of -2.8 to

-1.5 ppbv at the HT site, -3.0 to -2.3 ppbv at the Ryori site, and -2.3 to -0.7 ppbv at the Yona site.

3 Results

3.1 Simulated HONO and ClNO$_2$ and contributions from ship emissions

Figure 2a shows the horizontal distribution of the average HONO at the surface layer in the BASE case. The predicted HONO was widespread over the oceans, with mixing ratios ranging from 0.005 to 0.300 ppbv and distinct higher concentrations along the main shipping lanes. The distribution of HONO was consistent with that of NO$_2$ (Fig. S3) due to the heterogeneous conversion of NO$_2$ to form HONO and direct HONO emission from ships. In the vertical direction, the simulated HONO was concentrated at the surface and reached up to 400–600 m in the coastal and marine areas (see Fig. S4). Figure 3 shows the vertical profile of HONO from ship emissions in the nine selected regions. Consistent with the overall HONO vertical distribution, ship-contributed HONO also peaked at the surface in the oceanic areas, with average HONO levels of 3–120 pptv in the marine boundary layer (MBL). The greatest contribution of ship emissions was simulated in the WPO (96 %), followed by the SOJ (80 %), the BOB (49 %), the three Chinese waters (14 %–16 %), and the coastal cities (3 %–12 %). The varying ship contributions in these regions can be explained by the relative strength of the emissions from ships and from the adjacent land areas.

High values of ClNO$_2$ were simulated along the coasts and peaked in the lower MBL (Fig. 2b), with mixing ratios ranging from 2 to 400 pptv in oceanic areas and the highest value in the BR region. This distribution was in line with
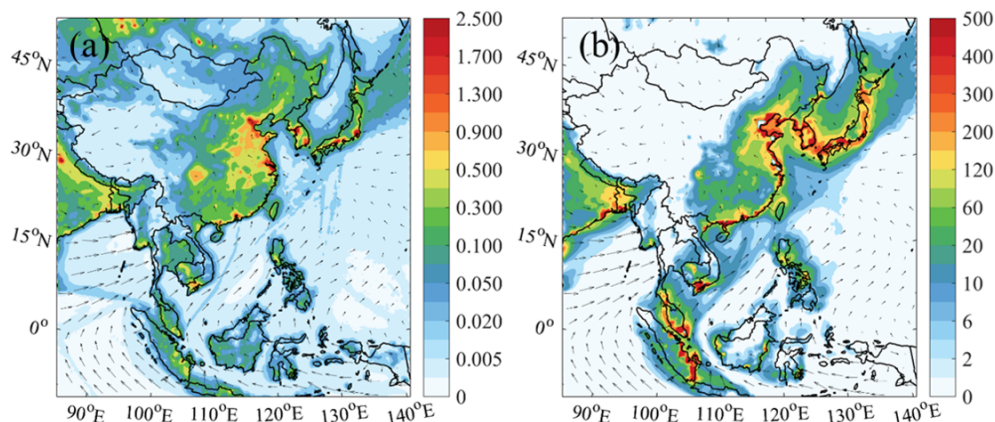
Figure 2. Spatial distributions of the simulation of averaged **(a)** HONO (in ppbv, whole day) and **(b)** night-time ClNO$_2$ (in pptv, 18:00–06:00 LST, local standard time) at the surface layer ($\sim$ 30 m) in July 2018 from the BASE case. The arrows present simulated wind vectors from the BASE case.
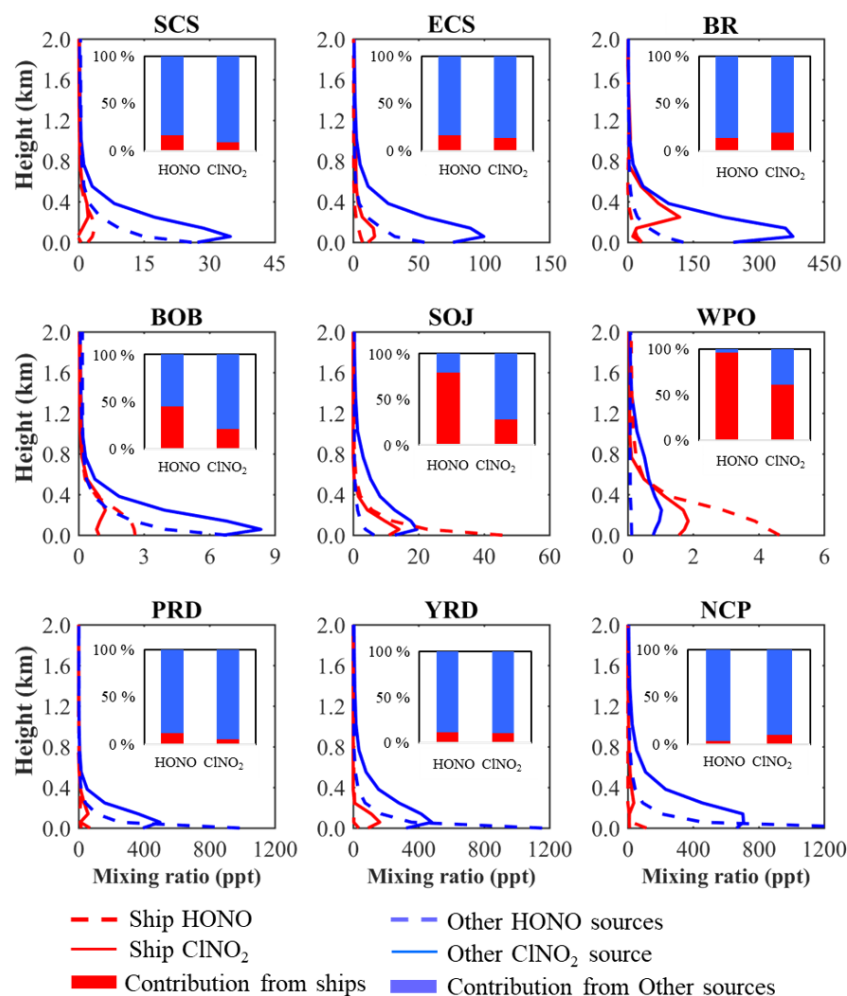

Figure 3. Vertical profiles of simulated HONO and night-time ClNO$_2$ (in ppt) from ship emissions and other sources in the nine regions. Also shown are the contributions of ship emissions and other sources to averaged HONO and night-time ClNO$_2$ levels in the marine boundary layer (within 600 m).

that of its precursors, N_2O_5 (Fig. S5) and particulate chloride (Fig. S6). Vertically, the peak value of $ClNO_2$ was simulated in the residual layer (100–300 m; Fig. 3), with mixing ratios of 8–350 pptv in oceanic areas. Similar to HONO, the greatest ship contribution to $ClNO_2$ was also simulated in the WPO (61 %), followed by other oceanic areas (9 %–24 %) and coastal cities (5 %–11 %).

We compared the modelled HONO and $ClNO_2$ with field observations made at some coastal and marine sites (see Table S4). The simulated HONO mixing ratios were 0.1–0.3 ppbv and 0.01–0.1 ppbv over the respective coastal BR and SCS sites and were comparable to the measurements at the marine sites of the BR (0.2 ppbv) (Wen et al., 2019) and SCS (89 pptv) (Table S4). For the coastal areas of other Asian countries, the simulated HONO compared well with the measurements in South Korea (0.60 ppbv) (Kim et al., 2015) and Japan (0.63 ppbv) (Takeuchi et al., 2013). HONO was simulated at approximately 5 pptv in the open ocean and 10–25 pptv along the main shipping lanes (Fig. 2a), which are values comparable to the measured HONO (3–35 pptv) in the open ocean in Europe and North America (Meusel et al., 2016; Kasibhatla et al., 2018; Ye et al., 2016). For $ClNO_2$, the order of magnitude and variation in the measured N_2O_5 and $ClNO_2$ levels at the HT site were reasonably reproduced by our model for early autumn of 2018 (Dai et al., 2020). The model performance of HONO and $ClNO_2$ in the land areas of mainland China for the summer of 2014 was also evaluated by L. Zhang et al. (2017). Overall, our model ability with respect to simulating HONO and $ClNO_2$ is acceptable, and the model results are sufficiently reliable for further analysis.

3.2 Impact of ship-derived HONO and chlorine on RO_x, O_3, and $PM_{2.5}$

In this section, we evaluate the ship effects on the main atmospheric radicals (RO_x, $OH + HO_2 + RO_2$), O_3, and $PM_{2.5}$ with the default chemistry (described in Sect. 2.3) and with the additional HONO and chlorine chemistry.

3.2.1 RO_x

Figure 4 shows the simulated differences in the average daytime RO_x mixing ratios at the surface from the cases with and without ship emissions using different chemistry. The RO_x mixing ratio was noticeably increased by ship emissions over oceanic areas, and this enhancement was magnified by the additional nitrogen chemistry. With the default chemistry (Fig. 4a), the average ship contribution to RO_x was about 18 % over the whole oceanic area. The addition of the HONO and chlorine chemistry increased the ship contributions to 28 % (Fig. 4b) and 22 % (Fig. 4c) respectively. Photolysis of ship-generated HONO and $ClNO_2$ released radicals (OH and Cl; Fig. S7) and recycled NO_x, which then oxidized VOCs and gave rise to high levels of RO_x. With the combined HONO and chlorine chemistry, the ship contribution

was further increased to 38 % (Fig. 4d). This combined ship contribution was smaller than the sum of that from the separate HONO and chlorine chemistry (22 % + 28 % = 50 %), which can be explained by the nonlinear interactions of the chemical system. Figure 5 shows the vertical profile of the RO_x mixing ratio from ship emissions in the nine regions. The enhanced RO_x reached an altitude of greater than 2 km over the oceanic regions, indicating the significant impact of ship-derived HONO and $ClNO_2$ on the oxidative capacity in the marine troposphere.

The largest increase in the ship contribution to RO_x was predicted in the WPO region (from 29 % to 50 %; Fig. 9a), followed by other oceanic areas (from 3 %–12 % to 6 %–17 %) and coastal cities (from −2 %–3 % to 4 %–6 %). The maximum ship contribution in the WPO region was consistent with the greatest ship contribution to HONO and $ClNO_2$ in this region (Fig. 4d). In the SCS and BOB regions, the enhanced RO_x was more dispersed with the combined nitrogen chemistry than that with the default and separate nitrogen chemistry. In the coastal cities, the RO_x mixing ratio was also affected by ship emissions via the transport of ship-generated HONO and $ClNO_2$ by summertime winds.

3.2.2 O_3

Figure 6 shows the simulated differences in the average O_3 at the surface from the cases with and without ship emissions. Consistent with the impact of ship emissions on oceanic RO_x, the oceanic O_3 was also noticeably increased (by 9 %) by ship emissions, which was further enhanced by the addition of HONO (12 %) and $ClNO_2$ (14 %) and combined nitrogen chemistry (21 %). The simulated distribution of ship-enhanced O_3 with the default chemistry was along the main shipping routes with high NO_x emissions (Fig. 6a). O_3 formation was highly sensitive to NO_x from ship emissions due to the relatively low concentrations of NO_x in the marine areas. The larger ship contribution with $ClNO_2$ chemistry than with HONO chemistry may be partially explained by a higher production ozone efficiency by NO_2 than by NO (from photolysis of HONO) and by the faster reaction rate of Cl radicals than OH radicals with long-lived alkanes.

With the combined impact from HONO and $ClNO_2$, widespread ozone increases were simulated over the SCS, BOB, and WPO regions (Fig. 6d). The combined nitrogen chemistry also increased the ozone concentrations in the coastal areas; in contrast, these concentrations were decreased by HONO or $ClNO_2$ separately. As shown in Fig. 6b and c, distinct ozone enhancement was simulated over the marine area of South Korea and Japan by HONO or $ClNO_2$. However, this enhancement was weakened and even cancelled by their combined effects. We calculated an indicator of the ozone formation regimes based on the ratio of the production rate of H_2O_2 to that of HNO_3 ($P_{H_2O_2}/P_{HNO_3}$) (Fu et al., 2020). Figure 7, with the combined HONO and $ClNO_2$ chemistry, shows that the NO_x-sensitive regime in East Asia
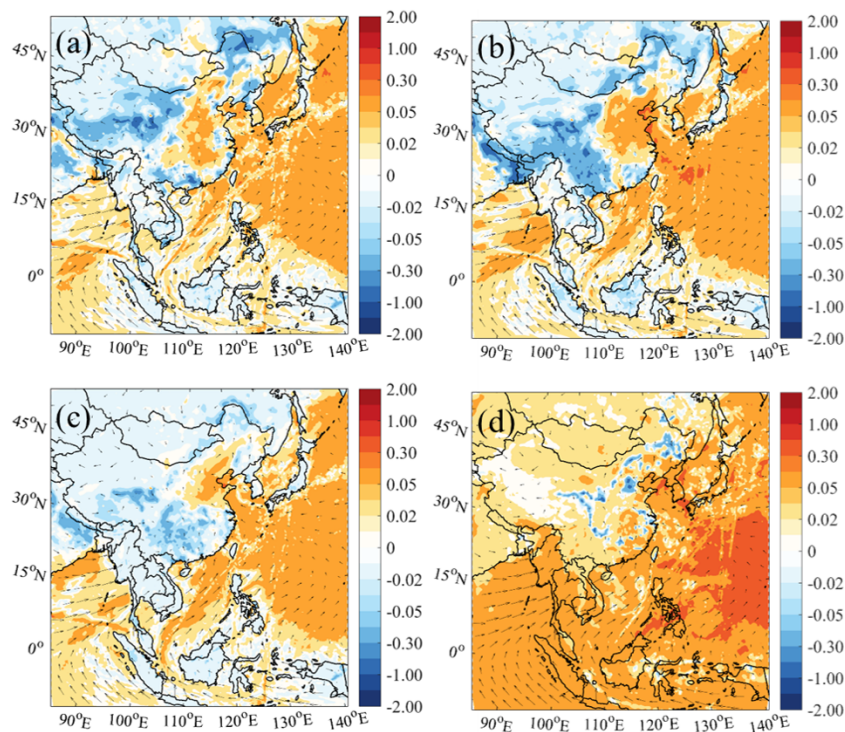
Figure 4. Averaged daytime RO$_x$ changes due to ship emissions (06:00–18:00 LST; in pptv) with **(a)** default chemistry (Def − Def_noship), **(b)** default and additional HONO chemistry (HONO − HONO_noship), **(c)** default and additional chlorine chemistry (Cl − Cl_noship), and **(d)** default and combined HONO and chlorine chemistry (BASE − BASE_noship). The arrows present simulated wind vectors from the BASE case.
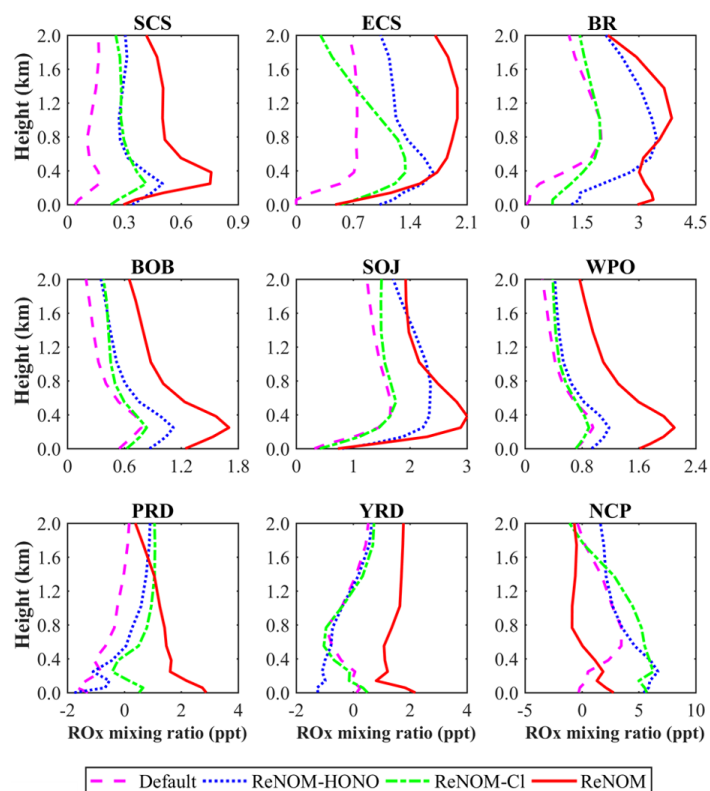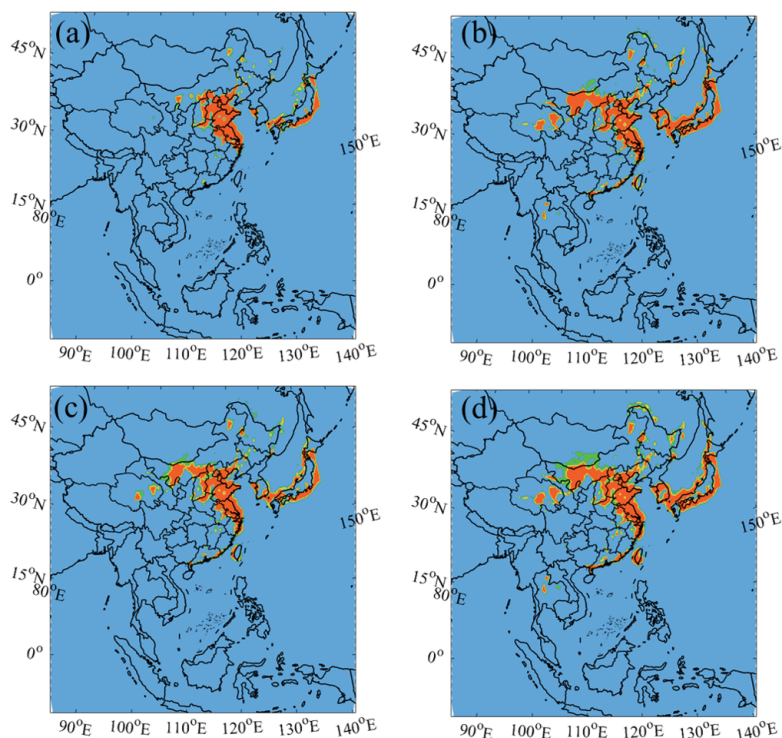

Figure 5. Vertical profiles of daytime RO$_x$ changes due to ship emissions (in pptv) from different chemistry in the nine regions.

Figure 6. The 24 h averaged ozone changes (06:00–18:00 LST; in ppbv) due to ship emissions with **(a)** default chemistry (Def − Def_noship), **(b)** default and additional HONO chemistry (HONO − HONO_noship), **(c)** default and additional chlorine chemistry (Cl − Cl_noship), and **(d)** default and combined HONO and chlorine chemistry (BASE − BASE_noship). The arrows present simulated wind vectors from the BASE case.

Figure 7. The O$_3$ sensitivity regimes using the **(a)** Def, **(b)** HONO, **(c)** Cl, and **(d)** the BASE cases. The classification of the ozone sensitivity regime is based on production rates of H$_2$O$_2$ to HNO$_3$, and $P_{H_2O_2}/P_{HNO_3}$ values of < 0.06, 0.06–0.2, and > 0.2 correspond to VOC-limited, transition, and NO$_x$-limited conditions respectively (Zhang et al., 2009).
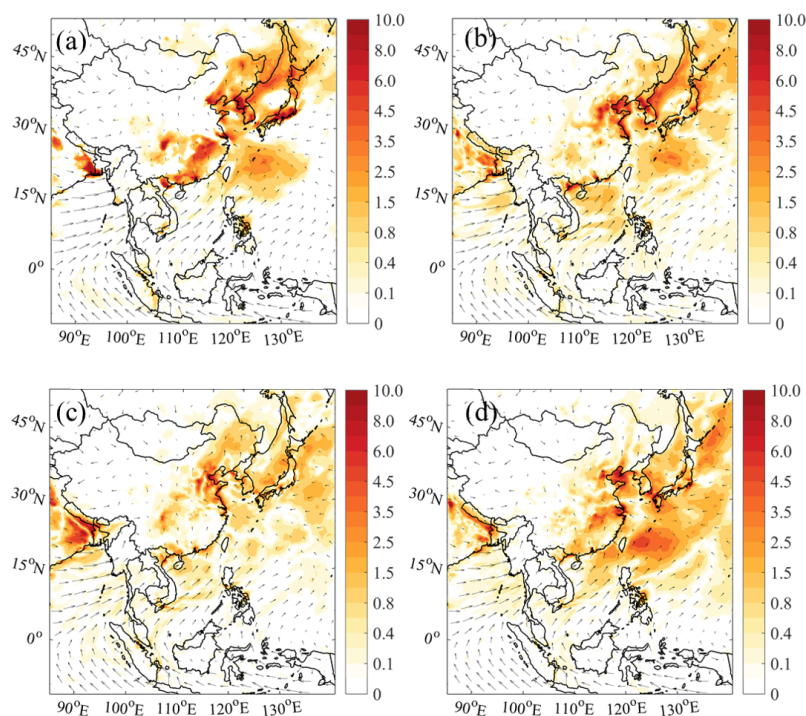
Figure 8. Averaged PM$_{2.5}$ enhancements due to ship emissions (in µg m^{-3}) with **(a)** default chemistry (Def − Def_noship), **(b)** default and additional HONO chemistry (HONO − HONO_noship), **(c)** default and additional chlorine chemistry (Cl − Cl_noship), and **(d)** default and combined HONO and chlorine chemistry (BASE − BASE_noship). The arrows present simulated wind vectors from the BASE case.

was changed to a VOC-sensitive regime, which was probably due to the increase level of NO or NO$_2$ from photolysis of HONO.

Figure S8 shows the vertical profile of ship-generated O$_3$ enhancement in the nine regions. Similar to ship-enhanced RO$_x$, ship-related O$_3$ enhancement stretched from the surface to the lower troposphere (> 2 km) over the marine regions. Because the emissions from ships occur at the sea surface, the vertically enhanced O$_3$ formation was caused by strong convection (Dalsøren et al., 2009).

The ship contribution to O$_3$ formation was also simulated in the WPO region (from 21 % to 38 %; Fig. 9b). Moreover, in other oceanic areas, the contributions of ship emissions were increased from 3 %–18 % to 12 %–24 %, with two distinct O$_3$ enhancements over the BR ($\sim$ 10 ppbv; Fig. 6d) and ECS (15 ppbv) regions. In the three coastal city clusters, the reduced O$_3$ formation was simulated by ship emissions with the default chemistry (from −5 to −1 ppb). Because these coastal cities are in the VOC-limited regime (Fig. 7a), the NO$_x$ from ships would lead to a decrease in chemical O$_3$ production. With the combined HONO and ClNO$_2$ effects, the ship-induced O$_3$ increased to −1 to −5 ppb due to the enhanced radicals and the transport of O$_3$ in the marine areas by ship-generated HONO and ClNO$_2$. The maximum O$_3$ increase in coastal cities also doubled from 3 ppb (5 %) to 7 ppb (11 %), aggravating the negative effects of ship emissions on human health in these regions.

In addition to the above coastal and oceanic areas, ship emissions also exert considerable impact on surface O$_3$ in distant inland areas such as the Sichuan Basin, and, interestingly, there are some "hot spots" of ozone (as well as RO$_x$, Fig. 4a–d, and PM$_{2.5}$, Fig. 8a–d) increase or decrease in the inland areas due to ship emissions (Fig. 6a–d). These hot spots may be a result of the inhomogeneous impact of ship emissions due to complicated dynamic and chemical processes that affect the fate and distribution of ship-emitted pollutants in the inland areas. In particular, the mountainous terrain in southern China may have large influence on the transport of ship emissions to inland areas.

3.2.3 PM$_{2.5}$

Ship-derived HONO and ClNO$_2$ also influence the production of aerosols via changes in radicals and NO$_x$. Figure 8 shows the simulated differences in the average PM$_{2.5}$ at the surface for cases with and without ship emissions. The PM$_{2.5}$ concentration was considerably enhanced by ship emissions, and the additional nitrogen chemistry further increased the simulated PM$_{2.5}$ concentration. With the default chemistry, the average ship contribution to the PM$_{2.5}$ concentration was about 7 % in oceanic areas (Fig. 8a), and it was increased to 10 % with the addition of HONO and ClNO$_2$ chemistry (Fig. 8d). The greatest contribution from shipping to the PM$_{2.5}$ concentration was also simulated over the WPO re-
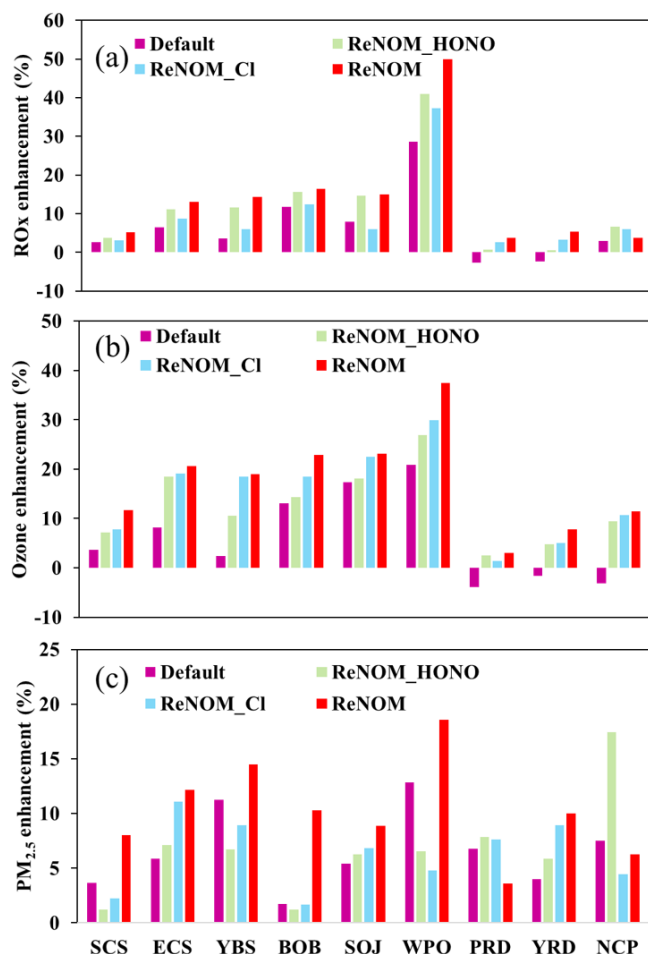
Figure 9. Contributions of ship emissions with different chemistry (Default, ReNOM_HONO, ReNOM_Cl, and ReNOM) to average mixing ratios of (**a**) daytime RO$_x$, (**b**) ozone, and (**c**) PM$_{2.5}$.

gion, as with ozone, with the contribution ranging from 13 % with the default chemistry to 19 % with the improved chemistry (Fig. 9c). In other oceanic areas, the ship contributions were also increased from 2 %–12 % to 6 %–15 %. We calculated the effects of ship-generated HONO and ClNO$_2$ on the formation of secondary particles. The additional ship HONO and chlorine chemistry increased the ship contribution to particulate nitrate from 13 % to 41 % in oceanic areas (Figs. S9 and S11) and its contribution to particulate sulfate from 11 % to 34 % (Figs. S10 and S11). In the coastal cities, the default contribution by ships was about 4 %–8 %, which was also increased to 4 %–12 % with the improved chemistry (Fig. 9c). The considerable increase in ship-contributed PM$_{2.5}$ and ozone due to HONO and ClNO$_2$ demonstrates the need to consider these compounds in evaluations of the impact of shipping on air quality.

Previous studies have evaluated the impact of ship emissions on the formation of O$_3$ and PM$_{2.5}$. Aksoyoglu et al. (2016) simulated the average ship contribution to oceanic

O$_3$ as 10 %–20 % in the Mediterranean area, and Huszar et al. (2010) showed a ship contribution of 10 % over the eastern Atlantic. The maximum O$_3$ enhancement by ship emissions was 15 ppb in the coastal waters of South Korea (Song et al., 2010) and 30–50 µg m^{-3} off the coast of the YRD region (Wang et al., 2019). For PM$_{2.5}$, the average ship contributions were about 20 %–25 % in European waters (Aksoyoglu et al., 2016) and 2.2 %–18.8 % off the coast of China (Lv et al., 2018).

Compared with previous studies, our study simulated a higher contribution to average ozone formation and a smaller contribution to average PM$_{2.5}$. We note that the underprediction of NO$_2$ in our simulation may lead to an underestimation of HONO, and the overpredicted PM$_{2.5}$ can result in an overestimation of N$_2$O$_5$ uptake, conversion of NO$_2$ to HONO, and production of ClNO$_2$. The exact effects of these uncertainties on the ozone and PM$_{2.5}$ is difficult to quantify. It is also difficult to discern the differences in our and previous modelling studies due to the differences in the methodologies adopted, including ship emission inventory, model resolution, chemical mechanisms (in addition to different treatment of HONO and ClNO$_2$ chemistry), and period of study. However, all of these studies demonstrate an important impact of ship emissions on atmospheric chemistry and air quality. The key finding of our study is the role of HONO and ClNO$_2$ in driving the oxidation processes, which has not been fully considered in most previous model studies of the impact of shipping on pollutant levels.

4 Conclusions

This study evaluated the production of HONO and ClNO$_2$ from international shipping and their impact on the oxidative capacity, ozone level, and level of fine PM in the maritime and coastal areas of eastern Asia. The results show that photolysis of the two compounds releases OH and Cl radicals, recycles NO$_x$, and changes conventional hydroxyl and organic peroxy radicals (RO$_x$ = OH + HO$_2$ + RO$_2$) by 0.8 %–21.4 % (0.8 %–7.7 % over coasts and 2.6 %–21.4 % over oceans), O$_3$ by 5.9 %–16.6 % (6.9 %–14.6 % over coasts and 5.9 %–16.6 % over oceans), and PM$_{2.5}$ by −1.2 %–8.6 % (−1.2 % to 6 % over coasts and 3.2 %–8.6 % over oceans) at the surface of the western Pacific regions. Their impact extends to the marine boundary layer. The largest contributions of HONO and ClNO$_2$ occur in the relatively remote oceans. Because ocean-going ships are a major source of NO$_x$, which is the key chemical precursor to HONO and ClNO$_2$, it is important to consider the sources and chemistry of these nitrogen compounds in evaluations of the impact of ship emissions.

References

Aksoyoglu, S., Baltensperger, U., and Prévôt, A. S. H.: Contribution of ship emissions to the concentration and deposition of air pollutants in Europe, Atmos. Chem. Phys., 16, 1895–1906, https://doi.org/10.5194/acp-16-1895-2016, 2016.

Andersson, C., Bergström, R., and Johansson, C.: Population exposure and mortality due to regional background PM in Europe – Long-term simulations of source region and shipping contributions, Atmos. Environ., 43, 3614–3620, https://doi.org/10.1016/j.atmosenv.2009.03.040, 2009.

Bertram, T. H. and Thornton, J. A.: Toward a general parameterization of N$_2$O$_5$ reactivity on aqueous particles: the competing effects of particle liquid water, nitrate and chloride, Atmos. Chem. Phys., 9, 8351–8363, https://doi.org/10.5194/acp-9-8351-2009, 2009.

Campling, P., Janssen, L., Vanherle, K., Cofala, J., Heyes, C., and Sander, R.: Specific evaluation of emissions from shipping including assessment for the establishment of possible new emission control areas in European Seas, Flemish Institute for Technological Research (VITO), Mol, Belgium, 2013.

Corbett, J. J. and Fischbeck, P.: Emissions from ships, Science, 278, 823–824, https://doi.org/10.1126/science.278.5339.823, 1997.

Corbett, J. J., Winebrake, J. J., Green, E. H., Kasibhatla, P., Eyring, V., and Lauer, A.: Mortality from ship emissions: a global assessment, Environ. Sci. Technol., 41, 8512–8518, https://doi.org/10.1021/es071686z, 2007.

Dai, J. N., Wang, X. M., Dai, W., and Chang, M.: The impact of inhomogeneous urban canopy parameters on meteorological conditions and implication for air quality in the Pearl River Delta region, Urban Climate, 29, 100494, https://doi.org/10.1016/j.uclim.2019.100494, 2019.

Dai, J. N., Liu, Y. M., Wang, P., Fu, X., Xia, M., and Wang, T.: The impact of sea-salt chloride on ozone through heterogeneous reaction with N$_2$O$_5$ in a coastal region of south China, Atmos. Environ., 236, 117604, https://doi.org/10.1016/j.atmosenv.2020.117604, 2020.

Dalsøren, S. B., Eide, M. S., Endresen, Ø., Mjelde, A., Gravir, G., and Isaksen, I. S. A.: Update on emissions and environmental impacts from the international fleet of ships: the contribution from major ship types and ports, Atmos. Chem. Phys., 9, 2171–2194, https://doi.org/10.5194/acp-9-2171-2009, 2009.

Devasthale, A., Krüger, O., and Graßl, H.: Impact of ship emissions on cloud properties over coastal areas, Geophys. Res. Lett., 33, 2, https://doi.org/10.1029/2005GL024470, 2006.

Eyring, V., Köhler, H., Van Aardenne, J., and Lauer, A.: Emissions from international shipping: 1. The last 50 years, J. Geophys. Res.-Atmos., 110, D17, https://doi.org/10.1029/2004JD005619, 2005.

Eyring, V., Isaksen, I. S., Berntsen, T., Collins, W. J., Corbett, J. J., Endresen, O., Grainger, R. G., Moldanova, J., Schlager, H., and Stevenson, D. S.: Transport impacts on atmosphere and climate: Shipping, Atmos. Environ., 44, 4735–4771, https://doi.org/10.1016/j.atmosenv.2009.04.059, 2010.

Finlayson-Pitts, B., Wingen, L., Sumner, A., Syomin, D., and Ramazan, K.: The heterogeneous hydrolysis of NO$_2$ in laboratory systems and in outdoor and indoor atmospheres: An integrated mechanism, Phys. Chem. Chem. Phys., 5, 223–242, https://doi.org/10.1039/B208564J, 2003.

Fu, X., Wang, T., Wang, S. X., Zhang, L., Cai, S., Xing, J., and Hao, J. M.: Anthropogenic emissions of hydrogen chloride and fine particulate chloride in China, Environ. Sci. Technol., 52, 1644–1654, https://doi.org/10.1021/acs.est.7b05030, 2018.

Fu, X., Wang, T., Zhang, L., Li, Q., Wang, Z., Xia, M., Yun, H., Wang, W., Yu, C., Yue, D., Zhou, Y., Zheng, J., and Han, R.: The significant contribution of HONO to secondary pollutants during a severe winter pollution event in southern China, Atmos. Chem. Phys., 19, 1–14, https://doi.org/10.5194/acp-19-1-2019, 2019.

Fu, X., Wang, T., Gao, J., Wang, P., Liu, Y., Wang, S. X., Zhao, B., and Xue, L.: Persistent Heavy Winter Nitrate Pollution Driven by Increased Photochemical Oxidants in Northern China, Environ. Sci. Technol., 54, 3881–3889, https://doi.org/10.1021/acs.est.9b07248, 2020.

Fuglestvedt, J., Berntsen, T., Eyring, V., Isaksen, I., Lee, D. S., and Sausen, R.: Shipping Emissions: From Cooling to Warming of Climate and Reducing Impacts on Health, Environ. Sci. Technol., 43, 9057–9062, https://doi.org/10.1021/es901944r, 2009.

Grell, G. A., Peckham, S. E., Schmitz, R., Mckeen, S. A., Frost, G., Skamarock, W. C., and Eder, B.: Fully coupled "online" chemistry within the WRF model, Atmos. Environ., 39, 6957–6975, https://doi.org/10.1016/j.atmosenv.2005.04.027, 2005.

Guenther, A., Karl, T., Harley, P., Wiedinmyer, C., Palmer, P. I., and Geron, C.: Estimates of global terrestrial isoprene emissions using MEGAN (Model of Emissions of Gases and Aerosols from Nature), Atmos. Chem. Phys., 6, 3181–3210, https://doi.org/10.5194/acp-6-3181-2006, 2006.

Gutzwiller, L., Arens, F., Baltensperger, U., Gäggeler, H. W., and Ammann, M.: Significance of semivolatile diesel exhaust organics for secondary HONO formation, Environ. Sci. Technol., 36, 677–682, https://doi.org/10.1021/es015673b, 2002.

Hoor, P., Borken-Kleefeld, J., Caro, D., Dessens, O., Endresen, O., Gauss, M., Grewe, V., Hauglustaine, D., Isaksen, I. S. A., Jöckel, P., Lelieveld, J., Myhre, G., Meijer, E., Olivie, D., Prather, M., Schnadt Poberaj, C., Shine, K. P., Staehelin, J., Tang, Q., van Aardenne, J., van Velthoven, P., and Sausen, R.: The impact of traffic emissions on atmospheric ozone and OH: results from QUANTIFY, Atmos. Chem. Phys., 9, 3113–3136, https://doi.org/10.5194/acp-9-3113-2009, 2009.

Huszar, P., Cariolle, D., Paoli, R., Halenka, T., Belda, M., Schlager, H., Miksovsky, J., and Pisoft, P.: Modeling the regional impact of ship emissions on NO$_x$ and ozone levels over the Eastern Atlantic and Western Europe using ship plume parameterization, Atmos. Chem. Phys., 10, 6645–6660, https://doi.org/10.5194/acp-10-6645-2010, 2010.

Kasibhatla, P., Sherwen, T., Evans, M. J., Carpenter, L. J., Reed, C., Alexander, B., Chen, Q., Sulprizio, M. P., Lee, J. D., Read, K. A., Bloss, W., Crilley, L. R., Keene, W. C., Pszenny, A. A. P., and Hodzic, A.: Global impact of nitrate photolysis in sea-salt aerosol on NO$_x$, OH, and O$_3$ in the marine boundary layer, Atmos. Chem. Phys., 18, 11185–11203, https://doi.org/10.5194/acp-18-11185-2018, 2018.

Keene, W. C., Khalil, M. A. K., Erickson III, D. J., Mcculloch, A., Graedel, T. E., Lobert, J. M., Aucott, M. L., Gong, S. L., Harper, D. B., and Kleiman, G.: Composite global emissions of reactive chlorine from anthropogenic and natural sources: Reactive Chlorine Emissions Inventory, J. Geophys. Res.-Atmos., 104, 8429–8440, https://doi.org/10.1029/1998JD100084, 1999.

Kim, S., Kim, S.-Y., Lee, M., Shim, H., Wolfe, G. M., Guenther, A. B., He, A., Hong, Y., and Han, J.: Impact of isoprene and HONO chemistry on ozone and OVOC formation in a semirural South Korean forest, Atmos. Chem. Phys., 15, 4357–4371, https://doi.org/10.5194/acp-15-4357-2015, 2015.

Kleffmann, J., Gavriloaiei, T., Hofzumahaus, A., Holland, F., Koppmann, R., Rupp, L., Schlosser, E., Siese, M., and Wahner, A.: Daytime formation of nitrous acid: A major source of OH radicals in a forest, Geophys. Res. Lett., 32, 5, https://doi.org/10.1029/2005GL022524, 2005.

Kurtenbach, R., Becker, K., Gomes, J., Kleffmann, J., Lörzer, J., Spittler, M., Wiesen, P., Ackermann, R., Geyer, A., and Platt, U.: Investigations of emissions and heterogeneous formation of HONO in a road traffic tunnel, Atmos. Environ., 35, 3385–3394, https://doi.org/10.1016/S1352-2310(01)00138-8, 2001.

Lawrence, M. G. and Crutzen, P. J: Influence of NO$_x$ emissions from ships on tropospheric photochemistry and climate, Nature, 402, 167–170, https://doi.org/10.1038/46013, 1999.

Li, M., Zhang, Q., Kurokawa, J.-I., Woo, J.-H., He, K., Lu, Z., Ohara, T., Song, Y., Streets, D. G., Carmichael, G. R., Cheng, Y., Hong, C., Huo, H., Jiang, X., Kang, S., Liu, F., Su, H., and Zheng, B.: MIX: a mosaic Asian anthropogenic emission inventory under the international collaboration framework of the MICS-Asia and HTAP, Atmos. Chem. Phys., 17, 935–963, https://doi.org/10.5194/acp-17-935-2017, 2017.

Li, Q., Zhang, L., Wang, T., Tham, Y. J., Ahmadov, R., Xue, L., Zhang, Q., and Zheng, J.: Impacts of heterogeneous uptake of dinitrogen pentoxide and chlorine activation on ozone and reactive nitrogen partitioning: improvement and application of the WRF-Chem model in southern China, Atmos. Chem. Phys., 16, 14875–14890, https://doi.org/10.5194/acp-16-14875-2016, 2016.

Liu, H., Fu, M., Jin, X., Shang, Y., Shindell, D., Faluvegi, G., Shindell, C., and He, K.: Health and climate impacts of ocean-going vessels in East Asia, Nat. Clim. Change, 6, 1037–1041, https://doi.org/10.1038/nclimate3083, 2016.

Liu, H., Jin, X., Wu, L., Wang, X., Fu, M., Lv, Z., Morawska, L., Huang, F., and He, K.: The impact of marine shipping and its DECA control on air quality in the Pearl River Delta, China, Sci. Total Environ., 625, 1476–1485, https://doi.org/10.1016/j.scitotenv.2018.01.033, 2018.

Liu, Y., Nie, W., Xu, Z., Wang, T., Wang, R., Li, Y., Wang, L., Chi, X., and Ding, A.: Semi-quantitative understanding of source contribution to nitrous acid (HONO) based on 1 year of continuous observation at the SORPES station in eastern China, Atmos. Chem. Phys., 19, 13289–13308, https://doi.org/10.5194/acp-19-13289-2019, 2019.

Lv, Z., Liu, H., Ying, Q., Fu, M., Meng, Z., Wang, Y., Wei, W., Gong, H., and He, K.: Impacts of shipping emissions on PM$_{2.5}$ pollution in China, Atmos. Chem. Phys., 18, 15811–15824, https://doi.org/10.5194/acp-18-15811-2018, 2018.

McDuffie, E. E., Smith, S. J., O'Rourke, P., Tibrewal, K., Venkataraman, C., Marais, E. A., Zheng, B., Crippa, M., Brauer, M., and Martin, R. V.: A global anthropogenic emission inventory of atmospheric pollutants from sector- and fuel-specific sources (1970–2017): an application of the Community Emissions Data System (CEDS), Earth Syst. Sci. Data, 12, 3413–3442, https://doi.org/10.5194/essd-12-3413-2020, 2020.

Meusel, H., Kuhn, U., Reiffs, A., Mallik, C., Harder, H., Martinez, M., Schuladen, J., Bohn, B., Parchatka, U., Crowley, J. N., Fischer, H., Tomsche, L., Novelli, A., Hoffmann, T., Janssen, R. H. H., Hartogensis, O., Pikridas, M., Vrekoussis, M., Bourtsoukidis, E., Weber, B., Lelieveld, J., Williams, J., Pöschl, U., Cheng, Y., and Su, H.: Daytime formation of nitrous acid at a coastal remote site in Cyprus indicating a common ground source of atmospheric HONO and NO, Atmos. Chem. Phys., 16, 14475–14493, https://doi.org/10.5194/acp-16-14475-2016, 2016.

Moldanová, J., Fridell, E., Popovicheva, O., Demirdjian, B., Tishkova, V., Faccinetto, A., and Focsa, C.: Characterization of particulate matter and gaseous emissions from a large ship diesel engine, Atmos. Environ., 43, 2632–2641, https://doi.org/10.1016/j.atmosenv.2009.02.008, 2009.

Monge, M. E., D'Anna, B., Mazri, L., Giroir-Fendler, A., Ammann, M., Donaldson, D., and George, C.: Light changes the atmospheric reactivity of soot, P. Natl. Acad. Sci. USA, 107, 6605–6609, https://doi.org/10.1073/pnas.0908341107, 2010.

Ndour, M., D'Anna, B., George, C., Ka, O., Balkanski, Y., Kleffmann, J., Stemmler, K., and Ammann, M.: Photoenhanced uptake of NO$_2$ on mineral dust: Laboratory experiments and model simulations, Geophys. Res. Lett., 35, 5, https://doi.org/10.1029/2007GL032006, 2008.

Osthoff, H. D., Roberts, J. M., Ravishankara, A., Williams, E. J., Lerner, B. M., Sommariva, R., Bates, T. S., Coffman, D., Quinn, P. K., and Dibb, J. E.: High levels of nitryl chloride in the polluted subtropical marine boundary layer, Nat. Geosci., 1, 324, https://doi.org/10.1038/ngeo177, 2008.

Sarwar, G., Simon, H., Xing, J., and Mathur, R.: Importance of tropospheric ClNO$_2$ chemistry across the Northern Hemisphere, Geophys. Res. Lett., 41, 4050–4058, https://doi.org/10.1002/2014GL059962, 2014.

Simon, H., Kimura, Y., Mcgaughey, G., Allen, D., Brown, S., Osthoff, H., Roberts, J., Byun, D., and Lee, D.: Modeling the impact of ClNO$_2$ on ozone formation in the Houston area, J. Geophys. Res.-Atmos., 114, D7, https://doi.org/10.1029/2008JD010732, 2009.

Song, S. K., Shon, Z. H., Kim, Y. K., Kang, Y. H., Oh, I. B., and Jung, C. H.: Influence of ship emissions on ozone concentrations around coastal areas during summer season, Atmos. Environ., 44, 713–723, https://doi.org/10.1016/j.atmosenv.2009.11.010, 2010.

Sun, L., Chen, T., Jiang, Y., Zhou, Y., Sheng, L., Lin, J., Li, J., Dong, C., Wang, C., and Wang, X.: Ship emission of nitrous acid (HONO) and its impacts on the marine atmospheric oxidation chemistry, Sci. Total Environ., 735, 139355, https://doi.org/10.1016/j.scitotenv.2020.139355, 2020.

Takeuchi, M., Miyazaki, Y., Tsunoda, H., and Tanaka, H.: Atmospheric acid gases in Tokushima, Japan, monitored with parallel plate wet denuder coupled ion chromatograph, Anal. Sci., 29, 165–168, https://doi.org/10.2116/analsci.29.165, 2013.

Tham, Y. J., Yan, C., Xue, L., Zha, Q., Wang, X., and Wang, T.: Presence of high nitryl chloride in Asian coastal environment and its impact on atmospheric photochemistry, Chinese Sci. Bull., 59, 356–359, https://doi.org/10.1007/s11434-013-0063-y, 2014.

Trinh, H. T., Imanishi, K., Morikawa, T., Hagino, H., and Takenaka, N.: Gaseous nitrous acid (HONO) and nitrogen oxides (NO$_x$) emission from gasoline and diesel vehicles under real-world driving test cycles, J. Air Waste Manage., 67, 412–420, https://doi.org/10.1080/10962247.2016.1240726, 2017.

UNCTAD: Review of Maritime Transport 2020, United Nations Publication, 159 pp., 2020.

Wang, R., Tie, X., Li, G., Zhao, S., Long, X., Johansson, L., and An, Z.: Effect of ship emissions on O$_3$ in the Yangtze River Delta region of China: Analysis of WRF-Chem modeling, Sci. Total Environ., 683, 360–370, https://doi.org/10.1016/j.scitotenv.2019.04.240, 2019.

Wang, T., Tham, Y. J., Xue, L. K., Li, Q. Y., Zha, Q., Wang, Z., Poon, S. C., Dubé, W. P., Blake, D. R., and Louie, P. K.: Observations of nitryl chloride and modeling its source and effect on ozone in the planetary boundary layer of southern China, J. Geophys. Res.-Atmos., 121, 2476–2489, https://doi.org/10.1002/2015JD024556, 2016.

Wen, L., Chen, T., Zheng, P., Wu, L., Wang, X., Mellouki, A., Xue, L. K., and Wang, W.: Nitrous acid in marine boundary layer over eastern Bohai Sea, China: Characteristics, sources, and implications, Sci. Total Environ., 670, 282–291, https://doi.org/10.1016/j.scitotenv.2019.03.225, 2019.

Ye, C., Zhou, X., Pu, D., Stutz, J., Festa, J., Spolaor, M., Tsai, C., Cantrell, C., Mauldin, R. L., and Campos, T.: Rapid cycling of reactive nitrogen in the marine boundary layer, Nature, 532, 489–491, https://doi.org/10.1038/nature17195, 2016.

Ye, C., Zhang, N., Gao, H., and Zhou, X.: Photolysis of Particulate Nitrate as a Source of HONO and NO$_x$, Environ. Sci. Technol., 51, 6849–6856, https://doi.org/10.1021/acs.est.7b00387, 2017.

Zaveri, R. A. and Peters, L. K.: A new lumped structure photochemical mechanism for large-scale applications, J. Geophys. Res.-Atmos., 104, 30387–30415, https://doi.org/10.1029/1999JD900876, 1999.

Zha, Q., Xue, L., Wang, T., Xu, Z., Yeung, C., Louie, P. K., and Luk, C. W.: Large conversion rates of NO$_2$ to HNO$_2$ observed in air masses from the South China Sea: Evidence of strong production at sea surface? Geophys. Res. Lett., 41, 7710–7715, https://doi.org/10.1002/2014GL061429, 2014.

Zhang, L., Wang, T., Zhang, Q., Zheng, J., Xu, Z., and Lv, M.: Potential sources of nitrous acid (HONO) and their impacts on ozone: A WRF-Chem study in a polluted subtropical region, J. Geophys. Res.-Atmos., 121, 3645–3662, https://doi.org/10.1002/2015JD024468, 2016.

Zhang, L., Li, Q., Wang, T., Ahmadov, R., Zhang, Q., Li, M., and Lv, M.: Combined impacts of nitrous acid and nitryl chloride on lower-tropospheric ozone: new module development in WRF-Chem and application to China, Atmos. Chem. Phys., 17, 9733–9750, https://doi.org/10.5194/acp-17-9733-2017, 2017.

Zhang, Y., Wen, X. Y., Wang, K., Vijayaraghavan, K., and Jacobson, M. Z.: Probing into regional O$_3$ and particulate matter pollution in the United States: An examination of formation mechanisms through a process analysis technique and sensitivity study, J. Geophys. Res.-Atmos., 114, D22, https://doi.org/10.1029/2009JD011900, 2009.

Zhang, Y., Yang, X., Brown, R., Yang, L., Morawska, L., Ristovski, Z., Fu, Q., and Huang, C.: Shipping emissions and their impacts on air quality in China, Sci. Total Environ., 581, 186–198, https://doi.org/10.1016/j.scitotenv.2016.12.098, 2017.